Noise from drones: Measurement, modelling and mitigation.

Ulf Orrenius [a)], Ulf Tengzelius [b)], Sacha Baclet [c)], Romain Rumpler [c)], Mats Åbom [c)] and Pernilla Ulfvengren [d)].

a) Akustikdoktorn Sweden AB
Drakens Gränd 6, II tr.
111 30 Stockholm, Sweden

b) Aurskall Akustik AB
Rute Hamnbacken 10,
624 58 Lärbro, Sweden

c) Marcus Wallenberg Laboratory, KTH 100 44 Stockholm, Sweden

d) INDEK,
KTH 100 44
Stockholm, Sweden

ulf@akustikdoktorn.se

Abstract

Drone noise is discussed with respect to measurements and characterization of emissions, modelling of noise footprints as well as noise mitigation by choice of vehicle design concept and route planning. It is shown how field-measured noise data can be used to derive acoustic source models with controlled uncertainty. Moreover, simplified physics-based models, based on e.g. vehicle mass and rotor properties are discussed in the context of extrapolating measured acoustic data at a given flight mode. Such models can also be used to support vehicle design optimization work regarding noise generation.

The newly developed SAFTu simulation platform provides a computationally efficient framework for analysing noise impact of drone traffic, or Urban Air Mobility (UAM). Ground noise is computed onto a moving grid using raytracing. The plotting of noise contours in $L_{A,MAX}$ or other metrics, typically only requires some CPU minutes. Starting from drone noise source models, flight paths and population data, calculation examples are presented illustrating how accurate UAM noise maps and population exposure statistics can be determined. Such maps can be used as a powerful planning and decision-making tool supporting the process of introducing novel drone traffic.

1 Introduction

Drones are becoming increasingly common. Today, professional drone operation is mainly limited to various types of surveying and inspection work, such as overflying of power lines or mapping storm damage and pests in forestry but, there are great expectations that drones will soon be able to perform different types of transport services, including airtaxi. Such services include transport to remote places as well as emergency medical transports to minimize the risk of delays due to traffic jams. Development of support services and infrastructure for drone flights is actively pursued at the EC [1] and national levels with the aim that drone services will contribute to increased mobility and reduced climate footprint.

2 Drones as noise sources

Predictive noise mapping from air traffic relies heavily on the assessment of the sound sources. Accurate source models are key to reliable calculation results on the ground. In programs like SAFTu [2], drone noise source strength and character representations must consider vehicle type and the associated flight modes. For the modelling of source strength, knowledge of rotor and operational parameters are useful, as discussed in Section 2.3 below.

2.1 Categorization of drones and VTOLs

Although a wide range of drone and air-taxi concepts are developing, as discussed in references [4] and [5], we here choose to categorize them into only two groups regarding their propulsion systems: VTOLs and multicopters. Within the group “multicopters” we address vehicles without wings, which use their rotors to generate both lift and thrust for forward propulsion. VTOL here denote a vehicle equipped with fixed wings for creating lift at level flight and rotors for lift generation at hover and vertical take-off and landing. Note that VTOLs either apply tilting rotors, so called proprotors, or two different sets of rotors/propellers to enable transitioning between level flight and vertical approach/take-off.

2.2 Source mechanisms

According to literature on UAM [4][5], future vehicle fleets are anticipated to be equipped with propellers or rotors powered by electric motors. As a result, flow induced rotor noise is expected to dominate the total noise emissions.

Based on physical mechanisms as described by the Ffowcs Williams and Hawkings equation [6], rotor noise can be classified into either thickness, loading or high-speed-impulsive noise, as illustrated in Figure 1. For drones and air-taxis with low-speed rotors (M<<1), high speed impulsive noise is generally not relevant. Blade loading noise is caused by variations in the aerodynamic forces on the rotor blades and was the first mechanism to be analysed and modelled [7]. Thickness noise is caused by the vortices created by the displacement of air mass from the blade motion.

Drone noise spectra typically consist of prominent tonal components in the low-to-mid frequency region, and broadband noise in the mid-to-high frequency region. The relative strength of the tonal noise increases with the number of rotor blades and rotor tip speed [7], but for small logistics drones, broadband noise typically dominates the total energy in the far-field [8] [9].

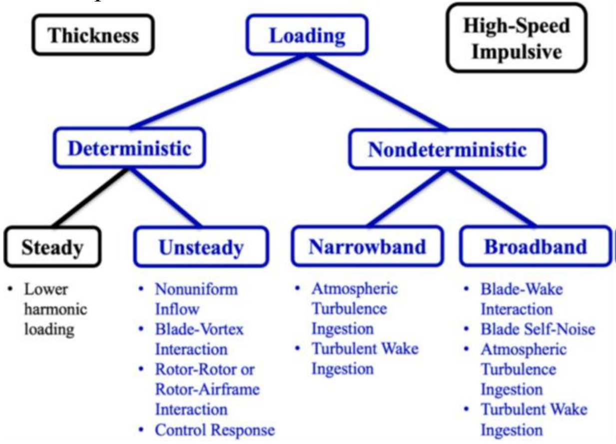

Figure 1. Rotor noise origin characterisation. From reference [5].

2.3 Physics-based noise models

The interest in future electrical aviation and UAM has substantially increased the research activities for rotor noise modelling [5][7][8] and associated noise abatement [4][5][10]. Models based on FWH equation, can be used to determine the frequency content of the generated noise and support rotor blade optimization. In relation to the governing physics and practical modelling needs, also early NASA work e.g. as reported in [11] is of interest, providing an overview of rotor noise physics and presenting applicable scaling laws for overall sound power generation,

$$L_w = 10\log\left(Av_{tip}^6\right) + 20\log(c_L) + c_1, \tag{1}$$

where v_{tip} is the rotor tip velocity, A is the (total) rotor area, c_L the total rotor blade lift coefficient integrated over all rotor sections and c_1 is a constant. Equation (1) has been experimentally validated for helicopters in reference [12] and for UAV rotorcraft in hover in ref. [13]. For derivation of Equation (1) it is assumed that loading noise dominates. It can be shown [15] that c_L is approximately proportional to the average geometrical pitch [13] [14], a property generally given by propeller manufacturers.

In addition, we have that the total rotor thrust can be written as,

$$T = 4c_T\rho A v_{tip}^2/\pi^3, \tag{2}$$

with c_T being the thrust coefficient and ρ the fluid density. The thrust coefficient is the integrated effect of the sectional lift coefficients across all rotor blades [15]. We can here assume that $c_T \sim Bc_L$ where B is the number of rotor blades.

In the far field, multicopter UAVs are somewhat directive when it comes to noise radiation, with the direction perpendicular to the rotor plane associated with the highest radiation [16]. This directivity is more pronounced at high frequencies. For large air taxi VTOLs, the *in-situ* hemisphere measurement approach [18], as developed for helicopter noise, can be used for source assessment, which provides directivity information but at a substantial cost.

For the needs of simulations, it is not judged to be reasonable to require directivity data for each type of Urban Aerial Vehicle (UAV). For some types of UAVs, directivity patterns can be estimated e.g. from generic directivity models derived for small multicopters [16][17] which can easily be incorporated into SAFTu and other prediction codes.

3 Measurement procedures

For modelling purposes, the apparent sound power radiated in different directions from the vehicle is needed, or expressed as the sound intensity projected on a sphere at a given radius. Although computational aeroacoustics (CAA) has developed greatly during the last decades [6], standardized measurement procedures with associated quality assessment methodology, are key to define source models and for certification purposes.

Source models are needed for all relevant modes of operation. For drones with fixed rotor systems which follows a vertical take-off and approach trajectory, these modes are: hover, level flight, take-off and approach. The EASA guidelines [20] for *in-situ* measurement of noise from UAVs up to 600 kg is an important step for realistic assessment of drone noise. Noise measurement at hover and at level overflight conditions are required but not at take-off and approach.

For VTOLs with rotor systems which can be tilted and/or with adjustable pitch rotors, there are more operational modes possible, in particular at approach and take-off. For such vehicles the procedures for deriving hemisphere source representation suggested by the NORAH project [18] may potentially be applied. In addition, based on ICAO procedures for heavy helicopters, EASA has published two so-called "consulting" Technical Specification papers [19] in which detailed descriptions for certification of air-taxi vehicles with tilting and non-tilting rotors are suggested. Also, maximum so called Effective Perceived Noise Levels (EPNL) are given as a function of Maximum Take-Off Mass (MTOM) for take-off, level overflight and approach reference procedures. No reference levels are given for the hover procedure.

3.1 Measurements according to EASA guidelines

3.1.1 Test execution

Sound levels from the KATLA3, a 40 kg MTOM logistics drone with two separate propulsion systems for lift and forward flight, were measured in October 2025 outside of Östersund. An NTI Audio XL2 sound level meter system, was used to record the audio signal. The sound level meter was calibrated before and after the measurement, with the sensitivity intact from the previous calibration.

The positioning of the UAS was taken from the KATLA3 internal GPS system, applying Satellite-Based Augmentation Systems with GNSS for increased precision. The altitude was also recorded. For the hover measurements, the altitude above ground level (AGL) was calculated from the reported altitude, subtracted with that recorded at the landing site.

The background noise level was measured before and after the measurements, with L_{AEQ} background levels being at least 20 dB below the measured sound level from the drone at overflight as well as at hover. The average wind speed at ground level was 2 m/s and at 60 m AGL 4 m/s.

3.1.2 Modes of operation

Four different modes of operation with 30 kg take-off mass were investigated: hovering at 17.5 m AGL and flying over the microphone setup at a height of 60 m AGL. For these measurements, the microphone was mounted inverted at 7 mm above a white and circular reflecting aluminium plate as required in the EASA guidelines [20] and shown in Figure 2. In addition, investigation measurements were made with the drone in vertical approach and take-off, with the microphone freely mounted in a flagpole at 10 m above ground level.

3.1.3 Applicable acoustic metrics

For the $L_{A,EQ}$ measured, the integration time was 30 s. for the EASA hover tests, 5 s. for the hover investigational tests and varied between 14 and 19 s. for the EASA overflight tests. For the $L_{A,MAX}$ sound level, the integration time was chosen as 1 s., i.e. the standard "slow" integration time for aircraft noise ($L_{AS,MAX}$). In addition, so-called $L_{AF,MAX}$ levels were recorded. Typically, the recorded difference $L_{AF,MAX}$ - $L_{AS,MAX}$ is 1-2 dB.

For the noise maps in the $L_{A,MAX}$ metrics we have chosen to use the measured $L_{AS,MAX}$ values for deriving source models, both at hover and at overflight modes. For a discussion on $L_{A,MAX}$ metrics for aviation noise, see e.g. reference [21].

Averages over six overflight and hover events were calculated. For the overflight measurements, the sound level was recorded during each flight. According to the EASA guidelines, also averaged sound exposure levels $L_{E,AVG}$ were calculated as,

$$L_{\mathrm{E,AVG}} = 10\log\left(\sum_i 10^{L_{E,i}/10}\right), \text{ with } L_{E,i} = L_{EQ,i} + 10\log(t_i), \quad (3)$$

where $L_{EQ,i}$ is the equivalent sound level of the i:th event, recorded over the measurement time t_i in seconds. Sound exposure levels (SEL) are typically used in combination with EPNL in aircraft certification [18] [22].

3.2 Source assessment at different operational modes

The EASA guidelines [20] from UAVs up to 600 kg requires *in-situ* measurement of noise at hover and at overflight conditions but not at take-off and approach, which is a limitation for modelling purposes. The increased sound generations at take-off may be estimated from hover data in combination with either test bench measurements, in which relationships thrust vs. sound power level are determined, or by applying scaling laws in combination with assumptions of the vertical acceleration. Correspondingly, at vertical approach the increase in maximum noise level is governed by the increase in thrust needed to reduce the vertical speed when approaching the ground [16].

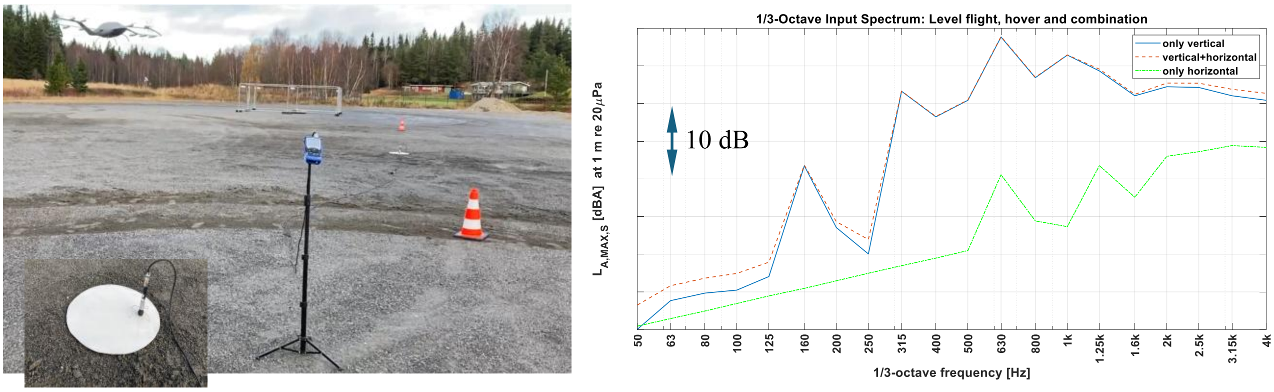

Figure 2. Left: Microphone arrangements for hover measurements. Right: Sound pressure level spectra at 1 m. from the KATLA3 for vertical, horizontal, and combined propulsion units. The spectra are tuned to field-measured overall levels.

For the UAV analysed, we have from Equation (1) together with Equation (2) that increasing rotor speed to provide a 10% increase in thrust from the hover level, results in about 1 dB increase in sound power. Such an increase in thrust results in realistic vertical acceleration, lifting the UAV to 50 m in 10 seconds, or an average climb rate of 5 m/s. Measured increase in L_{AMAX} for small UAVs during climb in relation to hover is in the same range, see e.g. reference [16]. Obviously, a higher climb rate would lead to more starting noise, and it is wise for operators to control the additional noise at take-off by applying a sensible climb rate. For descending small UAVs the increase of $L_{A,MAX}$ noise level relative to the hover level can be greater [16], associated with the increase in RPM needed to brake the vehicle before approach. So-called BVI noise, when rotor inflow is disturbed by self-generated vortices [2] may strongly contribute to the noise level as observed for helicopters in approach [12] and for UAVs with aerodynamically interfering rotors [13].

Alternatively, the measurement procedures for UAVs in approach or take-off as described in ISO/FDIS 5305:2024 [23] can be applied, although the recommended sound exposure level metrics ($L_{E,A,T}$) is not readily converted to the source power needed for modelling purposes. If available, $L_{A,MAX}$ levels recorded during vertical take-off and landing could be used as input to the source model. In this case, the shortest distance between the microphone and the vertical flight path should be used to estimate the sound power. Also, methodology for assessing of measurement errors and associated uncertainty is highly useful. Both in references [20] and [23], procedures for estimating measurement uncertainty are given, including that associated with measurement repeatability, UAV positioning accuracy, wind speed etc.

4 Calculation of noise on the ground

4.1 SAFTu software

The newly developed SAFTu simulation platform [2][3] provides a computationally efficient framework for analysing noise impact of drone traffic (UAM). The purpose is to enable noise exposure maps from general flying vehicles with specified trajectories under the conditions that:

- Runs/results should be easy to perform and understand also for inexperienced users
- Runs are “fast” on standard PC/laptops
- The software can be used as a stand-alone tool with minimal dependencies as far as possible.

SAFTu is based on its forerunner SAFT [24] and is written in and runs from within MATLAB®. Ground noise is computed using raytracing onto a moving grid underneath the vehicle. The calculations are limited to cover areas with significant noise levels, and the main output is noise contours representing, e.g. $L_{A,MAX}$-levels. The calculations are quick, typically requiring some CPU minutes depending on flight distance and on ground and building elevation data resolution.

Flight trajectories are created or read in, and noise maps can be produced for any geographic area on earth. This is enabled using free and open access supporting tools and data: Google Earth (GE) for manual ground track generation and results visualisation, QGIS and e.g. OpenTopography for elevation data handling and open data from sources such as Copernicus Global Digital Surface Model 30m. Other high resolution 3D data, including building geometries for increasingly more urban areas across the globe, are found in open sources or sources with some limited restricted access. Such data are usually directly applicable in SAFTu. Population data are taken from, e.g. OCHA /HDX and atmospheric profile data prognosis data from e.g. the Norwegian Meteorologic Institute, (Scandinavian/Baltic region) or simply a standard atmosphere. The vehicles are represented by their sound intensity at 1 m. The flight path is discretized in timesteps, typically around one second long.

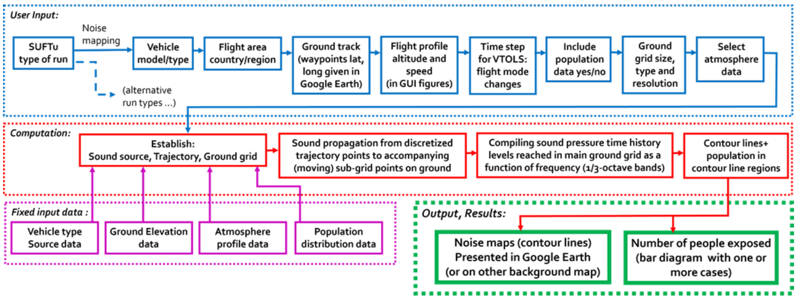

Figure 3. Process flow chart for a SAFTu run [2].

From the trajectory discretization points, the sound pressure at the ground grid points is currently computed using ray tracing with straight rays, and the sound pressure as a function of time, frequency and position is saved for each ground grid point with significant noise level. Noise histories are computed and $L_{A,MAX}$ and/or L_{AE} contour lines are plotted. Other noise metrics could easily be added. A self-explanatory interactive serial user input combined with fast runtimes enable an effective "learning by doing" process for new users [2][3]. Methods for refractive raytracing to assess noise in "shadow zones" or to account for cylindrical propagation due to atmospheric inversion conditions, are developed but not yet implemented in SAFTu.

4.2 Calculation examples

The first example is a 45 km flight simulation, Krokom- Föllinge in Jämtland as shown in Figure 4. To define source models for take-off and approach as well as for flyover, the $L_{AS,MAX}$ EASA test data from the 30 kg eVTOL presented in Section 3.1 and 3.2 is used.

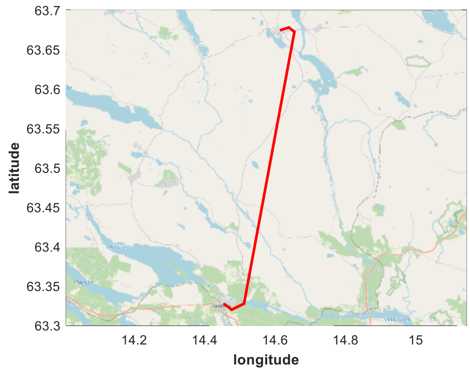

Figure 4. Flight path between Krokom and Föllinge (45 km)

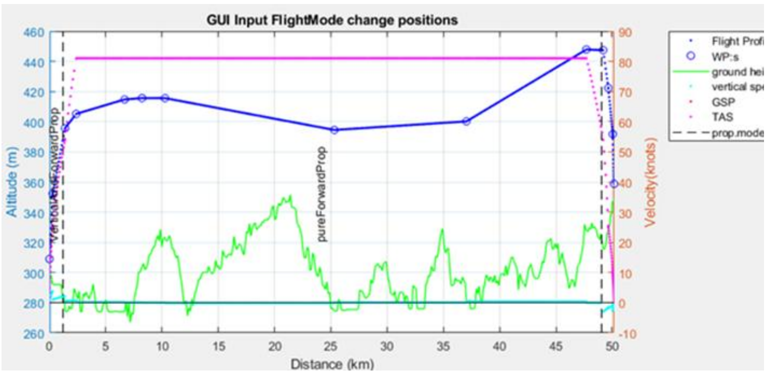

Figure 5. Flight mode input GUI in which the flight path is plotted above the ground height curve.

The ground track is here created by defining way points in Google Earth. Alternatively, the flight path and operational data are defined in an input CSV file.

Figure 6. Google Earth view of a flight trajectory with take-off in Högalidsparken, Stockholm.

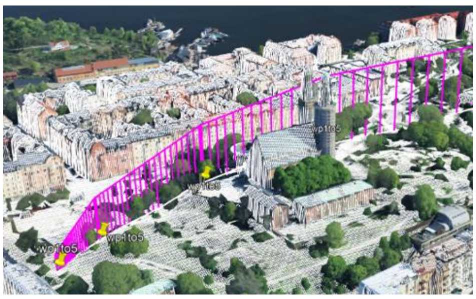

Figure 7. GE view with the ground grid shown as white lines including buildings and roads

In Figure 5, the finalised flight trajectory profile is shown, including the ground topography underneath. Positions for flight mode changes are indicated by dashed black lines: from copter to fixed-wing mode and vice versa.

For this example, the moving grid is re-sized to cover larger areas during take-off/landing (copter mode) than during en-route level flight (fixed-wing mode). In Figure 6 and Figure 7 a flight path at Södermalm in Stockholm is shown in which a software prototype for inclusion of buildings is used. In this second calculation example we apply laser scanned (LiDAR) data with resolution as fine as 1 m. In the calculation of the sound rays, diffraction according to the CNOSSOS-EU framework is applied in the vicinity of buildings. The source is in this case a generic air-taxi VTOL vehicle.

4.3 Results

In Figure 8, $L_{A,MAX}$ contours are shown for the Krokom take-off area as described above, and in Figure 9 a histogram graph representing the number of people living in different $L_{A,MAX}$ bands as defined by the noise map (for the entire route). In this case, a Digital Elevation Model (DEM) with a horizontal resolution of 30 m. was applied.

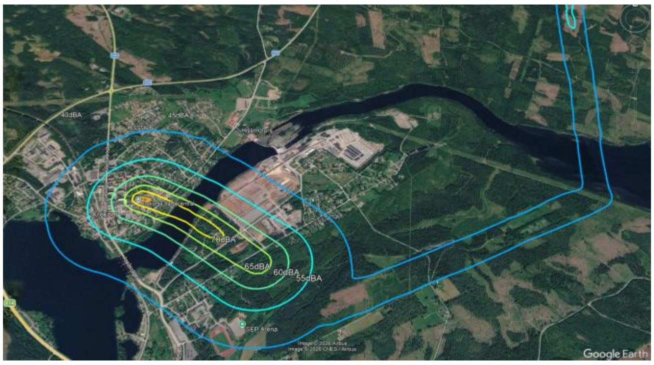

Figure 8. GE view with $L_{A, MAX}$ contours for the take-off site in Krokom.

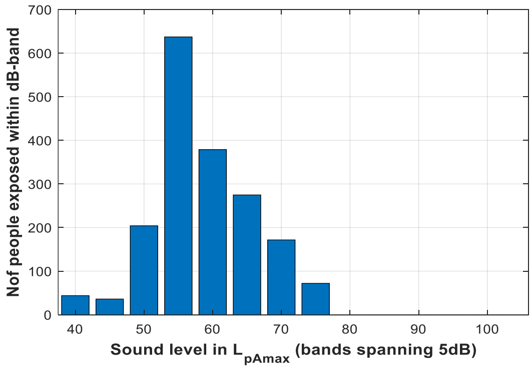

Figure 9. Noise exposure from Jämtland flight with no. of people living in $L_{A,MAX}$ bands.

In *Figure 10* and *Figure 11*, calculated $L_{A, MAX}$ contours are shown for the take-off area in Högalidsparken in Stockholm.

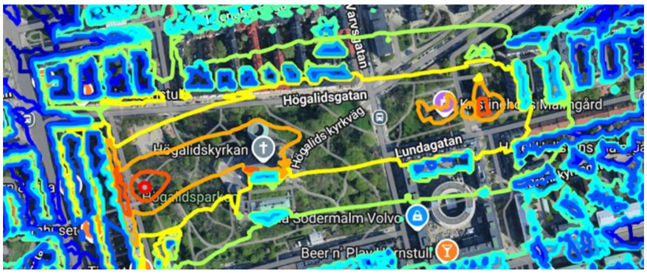

Figure 10. $L_{A,,MAX}$ noise contour maps in Google Maps.

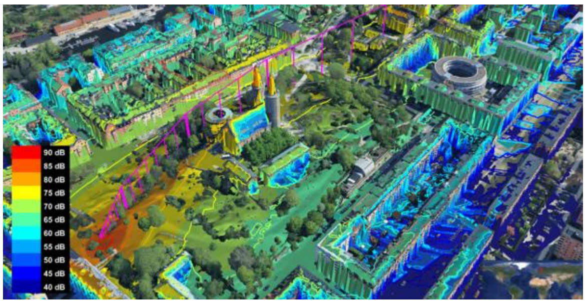

Figure 11. $L_{A, MAX}$ noise contour maps in GE with 3D rendering of buildings and vegetation.

Note that the circular building in the upper right corner of Figure 11 was not yet built at the time of the LiDAR data collection and is therefore not affecting the noise propagation simulated.

While other noise mapping tools are available, 3D rendering within the Google Earth framework is highly attractive for visualizing UAV noise. Topography is available globally as well as 3D building geometries in major cities. The widespread access to free DEM data further increases GE's appeal for presenting noise results.

5 Mitigation measures

5.1 Flight path planning and optimization

As illustrated by the noise maps most noise exposure is typically close to landing sites, and their location is likely to be the main noise concern for UAM implementation. Accordingly, the main interest in path optimization is typically related to the approach and take-off routing. Overflying drones can also be perceived as annoying, for example when loud multicopters are forced to fly at low altitude close to an airport. The results from SAFTu noise simulations can support decision-making and be used for communication of the expected noise exposure and effects of mitigation measures prior to implementation. It is generally wise to involve affected citizens early on, to explain benefits of the new transportation mode and measures taken to mitigate noise: use of low-noise UAVs, optimized flight routes, and measures on the infrastructure for example improved windows in facades.

For cities with high-rise buildings, detailed path planning along the flight routes is needed, and optimization schemes, combined with machine learning features can be a powerful aid in finding the best route regarding noise, ground risk and flight time [26][27]. When analysing the combined noise exposure from UAM and ground traffic, it is needed to account for the different source characteristics. The tonal spectra associated with rotor noise are typically perceived as more disturbing than spectra typical of traffic noise [25]. Also, it is generally not possible to control the exposure from UAM using barriers, and thus more difficult to offer noise shelter, a *quiet side*, at the side of a building opposite to the source.

5.2 Noise control at the source

Designers, developers and drone operators should be aware of how design choices affect noise generation. An informed choice of propulsion technology can support acceptance for a new drone service. For example, drones with wings can be made substantially more silent than those without [17]. Moreover, rotor size, blade pitch and rotor distance to the airframe and to adjacent rotors, are key parameters to noise generation [4][10]. The simple scaling law of Equation (1) is shown to reasonably well estimate the overall noise level of a UAV [13], and can together with the thrust model of Equation (2) and assessment of the thrust needed, be used for first estimates of acoustic source strengths for UAM noise exposure analysis. The models can also be used in conceptual design studies of rotor layout and choice of operation point.

With the thrust generated being proportional to $T\sim v_{tip}^2$, whereas overall noise generation follows $L_W\sim v_{tip}^6$, it is clear that reducing the rotor tip speed while keeping the thrust by, e.g., increasing the total rotor area A or the lift coefficient c_L, is generally beneficial for noise generation. Such measures also shift the tonal part of the spectrum to lower frequencies which is favourable when reduced A-weighted sound levels are sought. Increasing the number of rotor blades increases thrust [15] which can be exchanged for lower tip speed for reduced noise generation at equal thrust. Please note that increasing the number of blades will also shift the tonal part of the frequency spectrum to higher frequencies, which will increase A-weighted sound levels. Although outside of the scope for this short summary, rotor blade shape optimization is potentially fruitful e.g. by introducing so-called serrated trailing edges or bladelets. See e.g. references [8][10]. Moreover, rotors with adjustable rotor blade pitch offer advantages regarding noise generation, by tuning the operational point for minimized noise generation at a given thrust level [15].

6 Concluding remarks

Simulations are widely recognized for their role in supporting well-informed decision-making. By visualization of flight routes, simulation tools like SAFTu can effectively support the planning of suitable routes and the location of drone ports. Furthermore, calculation results can be integrated into various actors' processes for regulations, urban planning, traffic planning and not the least important, communication with affected citizens.

When purchasing drones, or UAM logistics services with a given routing and approach sites, noise simulation results can be used to set noise limits on the UAS systems, e.g. based on the EASA test standard. It is shown how simplified physics-based models, based on rotor properties such as tip speed, diameter, and pitch can be used to complement test data for source models derivation, and to support vehicle design optimization work regarding noise generation.

The simulation examples illustrate how both operational choices and the choice of UAV type for a certain flight route can greatly affect the noise exposure of the people living in the vicinity of the flight route and in particular the take-off and approach places. This means that the choices made in the set-up of a local UAM, concerning UAS system to be used, and the associated routing, can greatly contribute to the chances of success for future UAMs. To proactively manage noise exposure by low noise design of vehicles and their operations has the potential to remove negative connotations due to perceived annoyance for a particular drone type, but also for a particular drone service operating with a “noisy” drone.

When assessing drone noise in noise maps we have chosen to display levels calculated using the $L_{A,MAX,S}$ metrics, which are common to assess aircraft noise events. In relation to the ground traffic noise, research is needed in establishing relevant metrics for assessing acoustic disturbances from UAM traffic in relation to ambient sound [25].

7 Acknowledgement

The authors are grateful for the BEVIS project funding from Trafikverket and the DigiTools funding from AeroEDIH. The excellent collaboration with KATLA Aero AB during the Jämtland measurement campaign is also much appreciated.

8 References

[1] EU-kommission (2022). A drone strategy 2.0.

[2] Tengzelius, U., Orrenius, U. (2025), SAFTu user's manual v6.

[3] Tengzelius, U., Orrenius, U. (2025), SAFTu – A versatile noise mapping software for UAS or piloted flying vehicles., Proceedings of Inter-Noise 2025.

[4] Rizzi, S.A. et al. (2020), Urban Air Mobility Noise: Current Practice, Gaps, and Recommendations, NASA/TP–2020-5007433.

[5] Greenwood, E. et al., Challenges and opportunities for low noise electric aircraft, Int. J. of Aeroacoustics, 2022, Vol. 21(5-7) 315–338.

[6] Schram, C. and Roger, M. Review of aeroacoustic analogies and applications to urban air mobility, in book "Measurement, Modelling and simulations techniques for novel aircraft architectures", v. Karman Inst. 2024.

[7] Akiwate, D., On the balance between the tonal and broadband noise of isolated propellers, Int. J. of Aeroacoustics 2024, Vol. 23(1-2) 122–153.

[8] Sinibaldi, G. and Marino, L., Experimental analysis on the noise of propellers for small UAV. *Appl. Acoust.* 2013, *74, p.*79–88.

[9] Ramos-Romero, C. et al. (2023), On-field noise measurements and acoustic characterisation of multi-rotor small unmanned aerial systems. Aerospace Sci. Technol. 2023; 2023(141): 108 537.

[10] Candeloro, P. et al 2022. Small-scale rotor aeroacoustics for drone propulsion: a review of noise sources and control strategies, Fluids 7, 279.

[11] Marte, E. and Kurtz, D.W. 1970, A Review of Aerodynamic Noise From Propellers, Rotors, and Lift Fans, NASA Technical Report 32-7462.

[12] Schlegel, R. et al., Helicopter Rotor Noise Generation and Propagation, USAVLABS TR 66-4, Ft. Eustis, Va.,1966.

[13] Orrenius, U. et al., Towards accurate UAV source models for noise mapping, Proc. Quiet Drones, Delft, 2026.

[14] Storch, V. et al. Measurement of noise and its correlation to performance and geometry of small aircraft propellers**,** EPJ Web of Conferences, EPJ Web of Conferences, Volume 114, (2016) 02112

[15] Leishman, J. G. 2026. Introduction to Aerospace Flight Vehicles, Chapter 44 Aircraft propellers, ISBN 979-8-9852614-0-0.

[16] Heutschi, K. et.al 2021, Synthesis of real-world drone signals based on lab recordings, Acta Acust. 4 (6) 24.

[17] Orrenius, U. et al 2024, Noise simulation for UAM integration- Application to a health-care logistics system, in Proceedings of the 2024 DICUAM, Delft, The Netherlands, March 2024

[18] M. Tuinstra, et al, NORAH2 NOISE: Final report, EASA sept 2024 (link as of 9th of April 2026)

[19] EASA 2023/ EASA 2024, Environmental Protection Technical Specifications applicable to VTOL-capable aircraft powered by non-tilting/tilting rotors, Consulting Papers.

[20] EASA 2023. Guidelines on noise measurement of unmanned aircraft systems lighter than 600 kg. Operating in the specific category (low and medium risk)_rev1. European Union Aviation Safety Agency.

[21] Da Silva, R. et al., New method for helicopter noise mapping, *Proc. Internoise 2013.*

[22] ICAO Annex 16, Chapter 8 of Volume I, and associated Evaluation Method of Appendix 2.

[23] ISO/FDIS 5305 (2024) Noise measurements for UAS (unmanned aircraft systems).

[24] Tengzelius, U., Aircraft noise mapping code SAFT (link as of 9th of April 2026)

[25] Schäffer, B. et al (2021). Drone Noise Emission Characteristics and Noise Effects on Humans—A Systematic Review. *International Journal of Environmental Research and Public Health*, *18*(11), 5940.

[26] Chen, Y. et al (2026), Research on Path Planning Methods and Characteristics of Urban Unmanned Aerial Vehicles Under Noise Constraints. Drones, 10(3), 227.

[27] Wang, Y. et al. (2026), A review of noise-aware path planning for urban drone operations, Control Engineering Practice, Volume 169, 2026, 106750, ISSN 0967-0661.